ERJ
Engineering Research Journal
Faculty of Engineering
Minoufiya University

THE EGYPTIAN GEOID BY THREE INTEGRAL TECHNIQUES

Raaed Mohamed Kamel Hassouna

Department of Civil Engineering, Faculty of Engineering
Minoufiya University, Shebin El-Kom, Egypt

ABSTRACT:

In this study, a comparison was held among the Stokes, Hotine and Deflection-geoid formulae for gravimetric geoid modelling in Egypt, regarding the resulting statistical geoid features and accuracies. For this purpose, relevant 2' x 2' grids of gravity anomalies, gravity disturbances and vertical deflection components were input, yielding 2' x 2' detailed geoid models. The comparison showed that the Stokes and Hotine methods yielded practically the same geoid features and accuracy. The Deflection-geoid technique showed different geoid features and significantly better accuracy. The comparison of the three geoid solutions at independent GPS/Leveling control, showed that the mean and standard deviation of discrepancies, pertaining to the Deflection-geoid formula, are less by about 36% and 8%, respectively, compared to those relevant to the other two formulae. Therefore, the vertical deflections are recommended as homogeneous input data type in gravimetric geoid determination.

في هذا البحث تمت المقارنة بين طرق (Stokes) و (Hotine) و (Deflection-geoid) في حساب نموذج الجيوئيد ودقته للأراضي المصرية. حيث تم استخدام شذوذ الجاذبية، واضطراب الجاذبية وانحراف الرأسي عن العمودي كبيانات شبكية مدخلة للطرق الثلاث، على الترتيب. وقد أظهرت المقارنة نفس معالم ودقة الجيوئيد الناتجة من طريقتي (Stokes) و (Hotine)، بينما كانت معالم الجيوئيد الناتج من الطريقة الثالثة مختلفة والدقة أعلى بدرجة ملحوظة. فقد أظهرت المقارنة عند نقط (GPS) معلومة المنسوب ومستقلة أن المتوسط و الانحراف المعياري للفروق بين الجيوئيد المرصود والمحسوب بالطريقة الثالثة أقل بنسبة 36 % ، 8% ، على الترتيب، من القيم الناتجة باستخدام طريقتي (Stokes) و (Hotine). لذا يوصى باستخدام انحراف الرأسي عن العمودي كأرصاد متجانسة لحساب نموذج الجيوئيد.

Keywords: Integral formula - Hotine - Deflection-geoid

1. INTRODUCTION

The model approach can be considered a computationally efficient tool for gravimetric geoid modeling. Such approach is generally characterized by solving the geodetic boundary value problem (GBVP) using numerical integral formulae. In this respect, the most common technique is the Stokes' integral method, which leans on gridded gravity anomaly data as input for gravimetric geoid determination. This is known as the third (or Robin) GBVP. Such trend has been used, utilizing the simple assessment of gravity anomalies as a gravitational data type, which is based on the known orthometric heights of gravity data points. Another trend is the Neumann second GBVP, which leans on gravity disturbances as input. This is accomplished via the Hotine formula. Hotine's method for geoid determination is gaining popularity, since the development of GPS satellite positioning capability, which has facilitated the determination of ellipsoidal heights that are necessary for the computation of gravity disturbances [13]. Moreover, an additional integral model is the Deflection-geoid formula, which has been recently applied for gravimetric geoid determination [7].

Of course, all techniques for gravity field determinations are based on the unique mathematical relationships among the various anomalous features. The limitation could then be the availability of a particular data type. Therefore, it could apparently seem that, at least regarding the integral methods, unique geoid heights would result from the Stokes, Hotine and Deflection-geoid formula. Such hypothesis could be positively supported by the unique mathematical foundation of such integral techniques. However, another factor could give some advantage of a particular input data type, such as the statistical physical nature and the spectral content of the anomalous data type itself.

For instance, by definition, the vertical deflection components does not contain a zero-degree term [4], while the gravity anomalies are free from the first-degree coefficients. Moreover, the various gravimetric elements have different physical natures, regarding the smoothness or roughness of the data type under consideration [8]. The more the anomalous feature contains partial derivatives in its

relation to the disturbing potential, the more rough is it (or the more is the high frequency content inherent into it). In particular, the anomalous potential and geoidal heights could be considered as the smoothest features. Thus, the deflection components, gravity anomalies and gravity disturbances are relatively rougher in nature, as they represent the horizontal and vertical gradients of the anomalous potential, respectively.

Therefore, the aim of this study is formulated as follows. Beside the application of the Hotine and Deflection-geoid methods to the Egyptian Territory, it is intended to investigate the effect of the associated input gravity disturbances and deflection components on geoid determination accuracy, in comparison with Stokes formula that routinely utilizes gravity anomalies as input.

2. DATA PROCESSING

The straightforward application of integral formulae is based on an appropriate gridding of a particular scattered point data type, using an efficient interpolation technique. The available discrete gravity disturbance data, vertical deflection components and gravity anomaly data for Egypt suffers from the lack of regular distribution, enough coverage and suitable resolution. Therefore, in order to overcome this problem, the Least-Squares Collocation technique was firstly used to predict respective 2'x2' grids of predicted gravity anomalies, gravity disturbances, prime-vertical and meridian deflection components at the geoid, based on all available heterogeneous gravitational data in Egypt. These grids cover the region bounded by ($22° N \le \varphi \le 32° N$; $25° E \le \lambda \le 36° E$). The input data included scattered GPS/Lev. geoidal heights, gravity anomalies, gravity disturbances and vertical deflection components. The collocation solution was performed about the GRIM5-C1EGIT geopotential model [3], tailored to Egypt up to degree and order 650, according to the algorithm given by [12]. Moreover, Helmert's topographic effect was taken into consideration in the remove-restore procedure. The GTOPO30 digital elevation model [11], was utilized in order to account for the topographic effects of the various data types [2].

The residual gravity anomaly, gravity disturbance and deflection components grids are then input for the relevant integral techniques, in order to yield the associated residual geoidal height grids. The three solutions are performed, using a unified integration cap radius $\psi_0 = 1°$. Figure (1) through (4) show contour maps for the three input residual grids.

Such data preparation strategy guarantees that, apart from some inevitable noise, the prepared different data grids originate from the same observed local field data, which supplements the target comparison among the resulting three geoidal height solutions, relative to the WGS-84 reference ellipsoid.

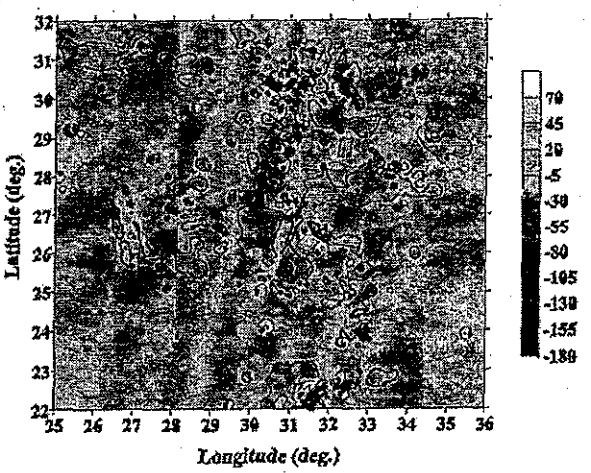

Figure (1): Contour map for the residual gravity anomalies (Interval: 25 mgals)

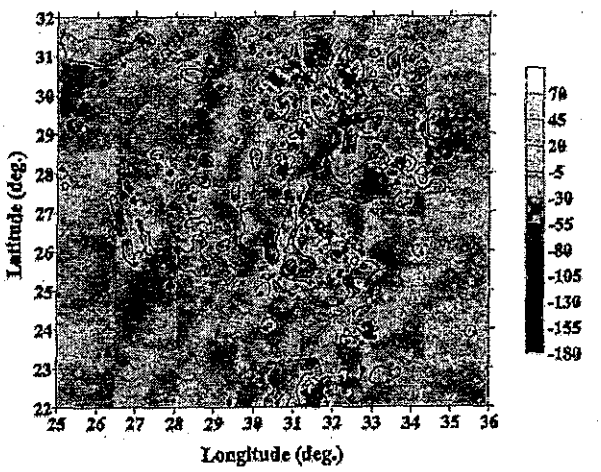

Figure (2): Contour map for the residual gravity disturbances (Interval: 25 mgals)

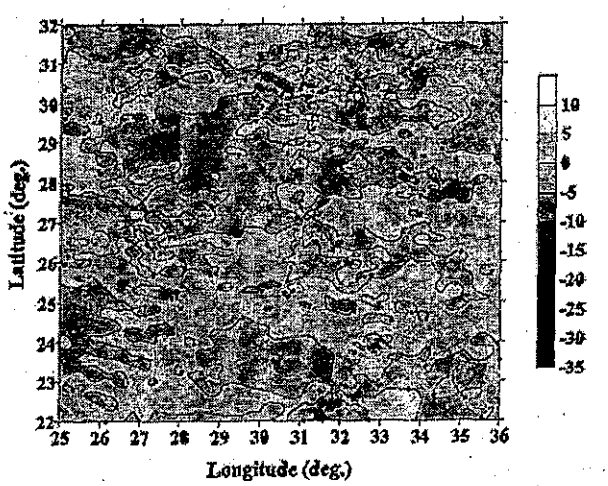

Figure (3): Contour map for the residual meridian deflections (Interval: 5 arc-second)

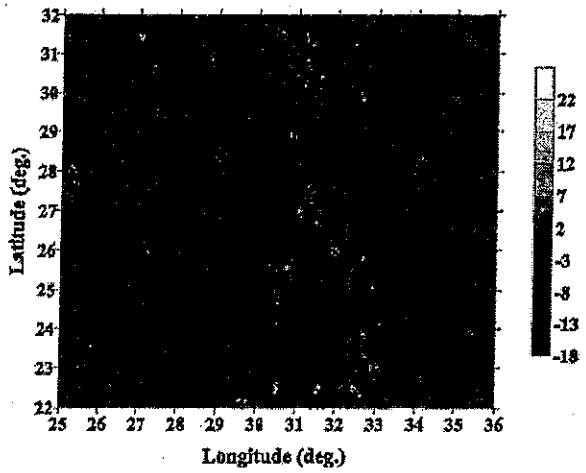

Figure (4): Contour map for the residual prime-vertical deflections (Interval: 5 arc-second)

3. COMPUTATIONAL PROCEDURES

Using spherical approximation and according to Stokes' formula, the geoidal height is computed at a certain point p, as follows

$$N_p = \left(R/4\pi\gamma_p\right)\iint_\sigma S\left(\psi_{pq}\right)\Delta g_q d\sigma \qquad (1)$$

where

R the mean radius of the Earth ($R \approx 6371$ km),

Δg_q the gravity anomaly (reduced to the geoid) at the running point q,

$S(\psi_{pq})$ the Stokes' kernel, given by;

$$S(\psi) = \operatorname{cosec}(\psi/2) - 6\sin(\psi/2) + 1 - 5\cos(\psi) - 3\cos(\psi)\ln\left[\sin(\psi/2) + \sin^2(\psi/2)\right] \qquad (2)$$

$D\varsigma$ the area element at the running point q,

γ_p the WGS-84 normal gravity, given as

$$\gamma_p = \left(a\gamma_e\cos^2\varphi_p + b\gamma_p\sin^2\varphi_p\right)/\sqrt{\left(a^2\cos^2\varphi_p + b^2\sin^2\varphi_p\right)} \qquad (3)$$

where a, b, γ_e and γ_p are the semi-major and semi-minor axis, equatorial and polar normal gravity, respectively, relevant to the WGS-84 reference ellipsoid, and ψ_{pq} the spherical distance between p and q, expressed as;

$$\cos\psi_{pq} = \sin\varphi_p\sin\varphi_q + \cos\varphi_p\cos\varphi_q\cos\left(\lambda_q - \lambda_p\right) \qquad (4)$$

Usually, the geoidal height is spectrally decomposed into three components, according to the relevant wavelengths, via the remove-restore technique. In particular, the far zone contribution is computed from the geopotential model (N_{GPM}). The near zone component (N^r) is provided by the local data within the limited integration cap centered at the computational point p. Finally, the detailed features are accounted for through the application of the topographic indirect effect, N^t, on the geoid [5]. Thus,

$$N = N_{GPM} + N^r + N^t \qquad (5)$$

Due to the discontinuous coverage of the gravitational data, even within the integration cap, the analytical integral in Eq. (1) is replaced by a numerical discrete summation. The discrete summation is more efficiently performed over a rectangular grid around the computation point. In the current study, the estimated residual geoidal heights is computed as follows;

$$N_p^r = \left(R/4\pi\gamma_p\right)\sum_\varphi\sum_\lambda \Delta g_q^r S\left(\psi_{pq}\right)\cos\varphi_q\Delta\varphi\Delta\lambda \qquad (6)$$

where $\Delta\varphi = \Delta\lambda = 2'$, Δg_q^r is the input residual gravity anomaly value at the running point q, and the summation is performed over a 1° cap around p.

Hotine formula computes the geoidal height in terms of gravity disturbances, δg, as follows [6]

$$N_p = \left(R/4\pi\gamma_p\right)\iint_\sigma H\left(\psi_{pq}\right)\delta g_q d\sigma \qquad (7)$$

where $H(\psi)$ is the Hotine kernel, given as

$$H(\psi) = \operatorname{cosec}(\psi/2) - \ln\left[1 + \operatorname{cosec}(\psi/2)\right] \qquad (8)$$

Again, given the residual gravity disturbances, δg^r, over the limited integration cap of radius 1°, the discrete Hotine summation yields the desired residual geoid undulation,

$$N_p^r = \left(R/4\pi\gamma_p\right)\sum_\varphi\sum_\lambda \delta g_q^r H\left(\psi_{pq}\right)\cos\varphi_q\Delta\varphi\Delta\lambda \qquad (9)$$

The Deflection-geoid formula solves for the geoid undulation in terms of the vertical deflection, as follows [7]

$$N_p = \left(R/4\pi\right)\iint_\sigma \Theta.dC\left(\psi_{pq}\right)/d\psi_{pq}d\sigma \qquad (10)$$

where Θ_α is the component of vertical deflection, at q, in the direction qp (having azimuth α_{qp}), which is assessed from

$$\Theta_\alpha = \xi_q\cos\alpha_{qp} + \eta_q\sin\alpha_{qp} \qquad (11)$$

ξ_q & η_q being the meridian and prime-vertical deflection components, respectively, at the running point q, and

$$\tan\alpha_{qp} = \left(-\cos\varphi_p.\sin\Delta\lambda_{pq}\right)/\left[2\sin\varphi_q.\cos\varphi_p.\sin^2\left(\Delta\lambda_{pq}/2\right) - \sin\Delta\varphi_{pq}\right] \qquad (12)$$

$C(\psi_{pq})$ is given by

$$C(\psi) = -2\log\sin(\psi/2) - 1.5\cos(\psi) - 1 \qquad (13)$$

and the Deflection-geoid kernel is

$$dC(\psi)/d\psi = -\cot(\psi/2) + 1.5\sin(\psi) \qquad (14)$$

Similarly, given the residual deflection components, ξ^r & η^r over a limited 1° integration cap, the discrete version of the Deflection-geoid integral gives the target residual geoidal height,

$$N_p^r = \left(R/4\pi\right)\sum_\varphi\sum_\lambda\left(\xi_q^r\cos\alpha_{qp} + \eta_q^r\sin\alpha_{qp}\right) dC\left(\psi_{pq}\right)/d\psi_{pq}.\cos\varphi_q\Delta\varphi\Delta\lambda \qquad (15)$$

Because a unified integration cap of radius 1° is used, the estimated three geoidal height grids were confined to the region ($23° N \le \varphi \le 31° N$; $26° E \le \lambda$

$\leq 35°$ E). This limited prediction region guarantees that no edge effects occur at the boundaries. Such effects would arise as a result of the incomplete integration caps at these domains. Having a resolution of 2' in both the latitude and longitude directions, such grid comprised 241 parallels of latitude and 271 meridians of longitude.

Regarding the three used techniques, the innermost zone effect was accounted for, by densifying the gridded data over an inner cap of size 1° around each computational point, via spline interpolation [10]. It is clear from Eqs (2), (8) and (14) that there exist inevitable singularities of the three integral formulae at the computation point. Therefore, the relevant geoid effect, δN_p, due to the data value at any computational point p, was accounted for in Stokes' technique, as follows [1]

$$\delta N_{strokes} = \left(\Delta g_p^r R/\gamma_p\right)\sqrt{\left(\Delta\varphi\Delta\lambda\cos\varphi_p/\pi\right)} \quad (16)$$

Similarly, in Hotine's method, this effect is assessed as [9]

$$\delta N_{Hotine} = \left(\delta g_p^r R/\gamma_p\right)\sqrt{\left(\Delta\varphi\Delta\lambda\cos\varphi_p/\pi\right)} \quad (17)$$

Regarding the Deflection-geoid technique, the corresponding value is given by [7]

$$\delta N_{Def.-geoid} = R^2\left(\xi_y^r + \eta_x^r\right)\left(\Delta\varphi\Delta\lambda\cos\varphi_p/4\pi\right) \quad (18)$$

where ξ^r_y & η^r_x are the horizontal gradients at p of the residual meridian and prime-vertical deflection components in the north and east directions, respectively.

Having estimated the residual geoid height grids, the long and short wavelength contributions are then restored back in order to obtain the final geoid undulation grids, according to Eq. (5). Therefore, the low frequency contribution was evaluated at the relevant grid nodes, using the harmonic expansion of the high resolution GRIM5-C1EGIT geopotential model [4],

$$N_{GPM} = \left(kM/r\gamma\right)\sum_{n=0}^{650}\left(a/r\right)^n\sum_{m=0}^{n}\left(\overline{C}^{*}_{mm}\cos m\lambda + \overline{S}_{mm}\sin m\lambda\right)\overline{P}_{nm}\left(\sin\theta\right) \quad (19)$$

with

- kM the geocentric gravitational constant,
- r the geocentric radius,
- γ the normal gravity induced by the WGS-84 reference ellipsoid (Eq. 3),
- a the equatorial radius scale factor associated with the harmonic model,
- θ the geocentric latitude,
- λ the geodetic longitude,
- $\overline{C}^{*}_{mm}$ the fully normalized spherical harmonic C-coefficients of degree n and order m, reduced for the even zonal harmonics of the WGS-84 reference ellipsoid,
- $\overline{S}_{mm}$ the fully normalized spherical harmonic S-coefficients of degree n and order m,
- $P_{nm}(\sin\theta)$ the fully normalized associated Legendre function of degree n and order m.

On the other hand, the high frequency geoid component, N^t, is accounted for via the application of the relevant geoid indirect effect at the grid nodes. In particular, the indirect effect of Helmert's second condensation reduction at a point p is given By

$$N_p^t = -\pi k\rho H_p^2/\gamma_p - \left(k\rho R^2/6\gamma_p\right).\sum\Delta\varphi\Delta\lambda\cos\varphi_q.\left(H_q^3 - H_p^3\right)/l^3 \quad (20)$$

with

- ρ Mean crustal density (taken 2670 kg/m^3),
- H_q Elevation of the running point q,
- H_p Elevation of the computation point p,
- L Spatial distance between p and q.

The above numerical integration was carried out for each grid node, up to a cap size of 0.75°, using the 30"x30" GTOPO30 model; and from 0.75° to 1.4°, using a 5'x5' coarser version of the same model.

4 RESULTS

Tables (1) and (2) show the statistics of the residual and final geoidal height grids, respectively, resulting from the Stokes, Hotine and Deflection-geoid formulae. One would agree that in general, the Stokes and Hotine solutions are very close and are somewhat different from those relevant to the Deflection-geoid solution. This fact is also manifested by Figure (5) through (7), which show the corresponding residual geoid contour maps. This is also reflected by the relevant final geoidal maps, which are plotted in Figure (8) through (10).

Table (1): Statistics of the residual geoidal height grids (unit: meter)

Technique	Mean	σ	RMS	Min.	Max.
Stokes	-0.012	0.294	0.294	-0.911	1.349
Hotine	-0.013	0.285	0.285	-0.911	1.314
Def.-geoid	0.003	0.220	0.220	-1.089	1.155

Table (2): Statistics of the final geoidal height grids (unit: meter)

Technique	Mean	σ	RMS	Min.	Max.
Stokes	14.210	2.804	14.484	5.817	21.531
Hotine	14.209	2.805	14.484	5.809	21.544
Def.-geoid	14.225	2.881	14.514	5.206	22.109

In order to compare the accuracies of the three geoid solutions, relevant residual geoid undulation values were estimated at 35 evenly distributed discrete GPS/Levelling check points, using respective integration caps at these scattered points. Then, the low and high frequency contributions, according to Eq. (19) and (20), respectively, were restored to the predicted residual geoidal heights at those discrete points.

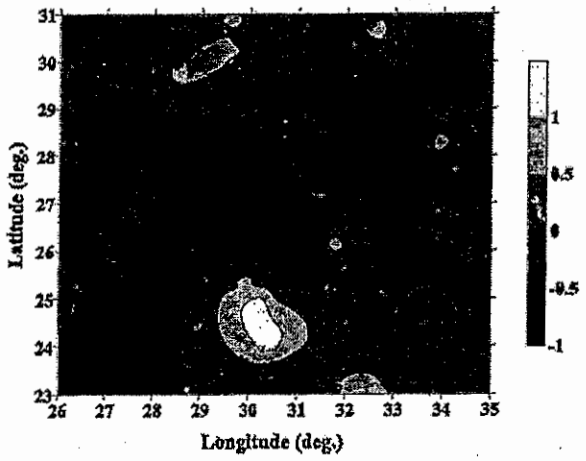

Figure (5): Stokes residual geoid contour map (Interval: 0.50 m)

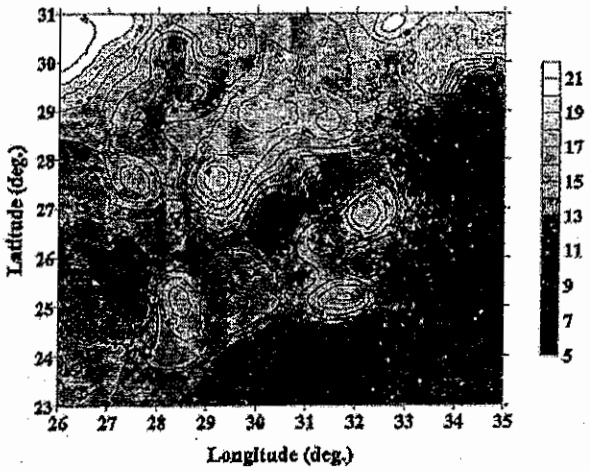

Figure (8): Stokes final geoid contour map (Interval: 1 m)

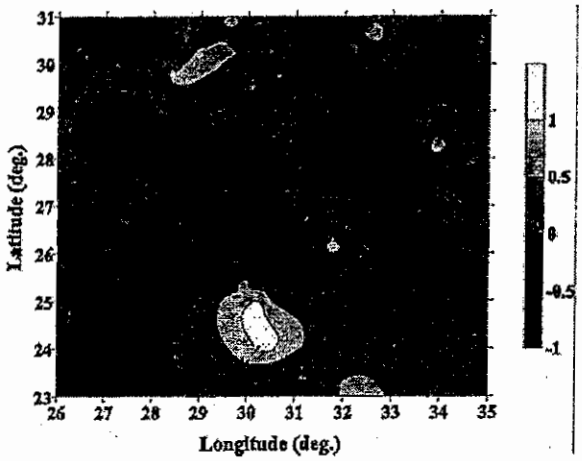

Figure (6): Hotine residual geoid contour map (Interval: 0.50 m)

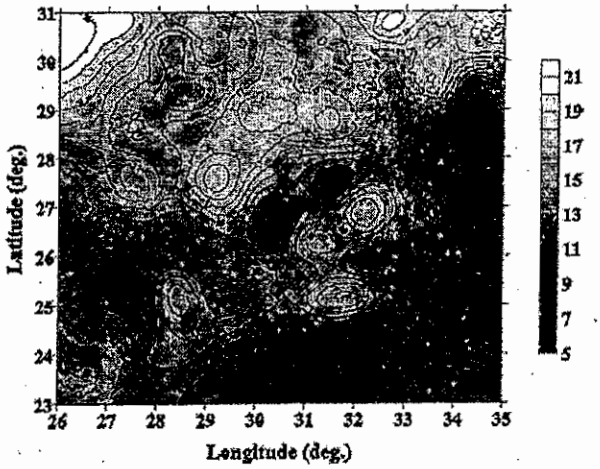

Figure (9): Hotine final geoid contour map (Interval: 1 m)

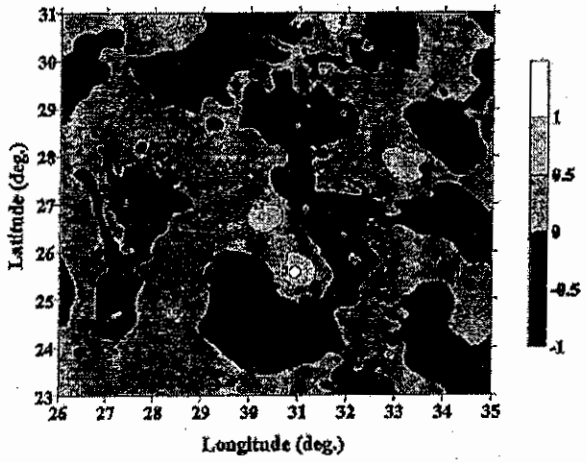

Figure (7): Def.-geoid residual geoid contour map (Interval: 0.50 m)

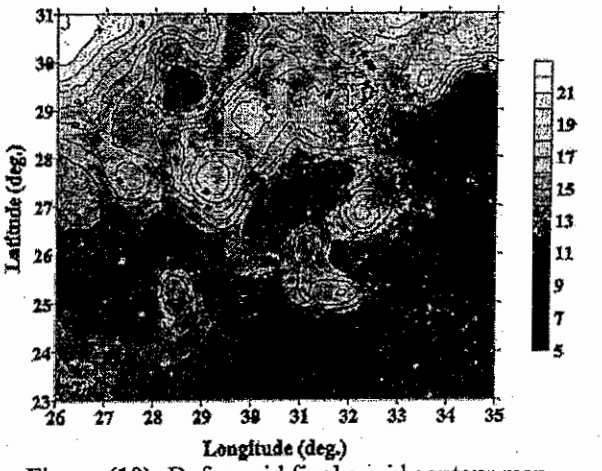

Figure (10): Def.-geoid final geoid contour map (Interval: 1 m)

Table (3) shows the statistics of the discrepancies between the GPS/Lev. geoid and the relevant gravimetric geoid values. Again, the Stokes and Hotine solutions have practically the same accuracy, and this is also true for the minimum and maximum differences. Surprisingly, the Deflection-geoid solution seems to be significantly more accurate than the two former solutions. In particular, the mean and standard deviation of discrepancies, relevant to the Deflection-geoid formula, are less in magnitude by about 36% and 8%, respectively, than those relevant to the other two formulae. Moreover, the magnitudes of the minimum and maximum discrepancy are less by about 8% and 14%, respectively, compared to the other two solutions. It should be noted that theoretically, the three solutions should have given the same results.

Table (3): Comparison of the three geoid solutions at GPS/Lev. check points (unit: meter)

Technique	Mean	σ	RMS	Min.	Max.
Stokes	-0.293	1.239	1.256	-2.699	3.176
Hotine	-0.291	1.235	1.252	-2.694	3.165
Def.-geoid	-0.187	1.136	1.135	-2.469	2.724

5 CONCLUDING REMARKS

Based on the used local field data, it can be concluded that the Deflection-geoid method results in a more accurate geoid model, compared to both the Stokes and Hotine techniques. In other words, the vertical deflection data type results in geoid prediction accuracy, which are considerably better than those relevant to gravity anomalies or gravity disturbances as input data types. The Stokes and Hotine geoidal features and accuracy are practically identical, which indicate that gravity anomalies and gravity disturbances could be considered as mutually equivalent data types. On the other hand, the vertical deflection components behave more efficiently during their use in geoid modelling. This could be attributed to the relatively medium roughness of such data, being the horizontal gradient of the disturbing potential, compared to the rougher gravity anomalies and disturbances.

Therefore, one could expect that the input grids of deflection components, although having the same spatial resolution as the input anomaly and disturbance grids, may have behaved as if it were of a relatively higher resolution, due to its medium spatial variability. In other words, a vertical deflection grid of lower spatial resolution could have resulted in an accuracy, which resembles the Stokes and Hotine's results in the current study. Another advantage of merely using vertical deflection components in geoid modelling is that they are by definition free from the zero-degree term uncertainty, which is inherent into any other data type. Therefore, using the vertical deflections may be recommended as input data type for geoid modelling.

6. REFERENCES

[1] Featherstone, W.E. and J.G. Olliver (1994): "A New Gravimetric Determination of the Geoid of the British Isles", *Survey Review*, 32, 254, October, pp: 464-478.

[2] Forsberg, R. and C.C. Tscherning, (1981): "The Use of Height Data in Gravity Field Approximation by Collocation", *Journal of Geophysical Research*, Vol. 86, No. 89, pp: 7843-7854.

[3] Gruber, T., A. Bode, Ch. Reigber, P. Schwintzer, R. Biancale and J.-M. Lemoine (2000): "GRIM5-C1: Combination solution of the global gravity field to degree and order 120", Geophysical Research Letters 27: 4005-4008.

[4] Heiskanen, W.A. and H. Moritz (1967): "Physical Geodesy", *W.H. Freeman and Company*.

[5] Higgins, M.B., M.B. Pearse and A.H.W. Kearsley (1996): "Using Digital Elevation Models in the Computation of Geoid Heights", *Geomatics Research Australasia*, No. 65 December, pp: 59-74.

[6] Hotine, M. (1969): "Mathematical Geodesy", *ESSA Monograph 2, U.S. Dep. Of Commerce*, Washington.

[7] Hwang, C. (1998): "Inverse Vening Meinesz formula and Deflection-geoid formula: applications to the predictions of gravity and geoid over the South China Sea", *Journal of Geodesy*, 72, pp: 304-312.

[8] Meissl, P. (1971): "A study of covariance functions related to the Earth's disturbing potential", *Report No. 151, Department of Geodetic Science*, The Ohio State University.

[9] Serpas, J.G. (2003): "Local and Regional Geoid Determination from Vector Airborne Gravimetry", *Report No. 468, Department of Civil and Environmental Engineering and Geodetic Science*, The Ohio State University.

[10] Tscherning, C.C., R. Forsberg and P. Knudsen (1994): "GRAVSOFT – A System for Geodetic Gravity Field Modelling", *Technical Note, 4th ed January, Department of Geophysics*, University of Copenhagen, Denmark.

[11] USGS (2000): "GTOPO30", *http://www.cr.usgs. gov /glis/hyper/ guide/gtopo30.*

[12] Wenzel, G. (1998): "Ultra High Degree Geopotential Model GPM3E97A to Degree and Order 1800 tailored to Europe", *Paper presented in Proceedings of 2nd Continental Workshop on the Geoid in Europe*, March 10-14, Budapest.

[13] Zhang, C. (1998): "Estimation of dynamic ocean topography in the Gulf Stream area using the Hotine formula and altimetry data", *Journal of Geodesy*, 72, pp: 499-510.